Biogeochemical drivers of methane dynamics in the water column of Georgian Bay's embayment, Lake Huron

Khoren Avetisyan,1* Xiaoqing Shao,1 David Sweetnam,2 Maria Dittrich1

¹Department of Physical and Environmental Sciences, University of Toronto Scarborough, Toronto; ²Georgian Bay Forever, Toronto, ON, Canada

ABSTRACT

Methane (CH₄) production in oxygenated freshwater systems remains an active area of research in biogeochemistry. This study investigates CH₄ dynamics in Honey Harbour's North Bay, a stratified freshwater oligotrophic embayment of Georgian Bay (Lake Huron), by integrating microbial community analyses, and geochemical measurements. The field study was conducted in 2021, with four sampling campaigns carried out during the months of July, August, September, and October. During stable stratification, CH₄ is present in oxic surface water with a maximum of 4.69 μg/L in September. The abundance of *Synechococcus* in surface waters indicates that CH₄ formation may be driven by methylphosphonate (MPn) degradation under phosphorus limitation conditions. Additionally, methanogenic archaea were detected in oxic waters, indicating possible methanogenesis in oxic surface freshwaters. The CH₄ oxidation possibly was supported by Fe- and Mn-reducing bacteria such as *Geothrix* and *Methylobacter*, which increased at depths below chemocline. Redundancy analysis (RDA) demonstrated strong positive correlations between CH₄, photosynthetically active radiation (PAR), and microbes linked to CH₄ cycling. Our study shows that CH₄ production in surface waters is influenced by phototrophic and archaeal activity, whereas deeper waters exhibit CH₄ oxidation coupled to metal cycling and Fe- and Mn-reducing bacteria. This study provides novel insights into microbial and geochemical interactions regulating CH₄ emissions in oligotrophic freshwaters of Georgian Bay embayment.

*Corresponding author: khoren.avetisyan@utoronto.ca

Key words: Laurentian Great Lakes; Georgian Bay; methane; oxic waters; iron; manganese.

Citation: Avetisyan K, Shao X, Sweetnam D, Dittrich M. Biogeochemical drivers of methane dynamics in the water column of Georgian Bay's embayment, Lake Huron. *J Limnol* 2025;84:2215.

Edited by: Cristiana Callieri, CNR-IRSA Water Research Institute, Verbania-Pallanza, Italy.

Contributions: MD, conceptualization, project administration, funding acquisition, supervision; MD, KA, methodology, data curation, manuscript original drafting; MD, KA, XS, DS, field investigation, manuscript review and editing; KA, XS, data and laboratory analysis. All authors read and approved the final version of the manuscript and agreed to be accountable for all aspects of the work.

Conflict of interest: the authors declare that they have no competing interests, and all authors confirm accuracy.

Received: 9 February 2025. Accepted: 7 August 2025.

Publisher's note: all claims expressed in this article are solely those of the authors and do not necessarily represent those of their affiliated organizations, or those of the publisher, the editors and the reviewers. Any product that may be evaluated in this article or claim that may be made by its manufacturer is not guaranteed or endorsed by the publisher.

°Copyright: the Author(s), 2025 Licensee PAGEPress, Italy J. Limnol., 2025; 84:2215 DOI: 10.4081/jlimnol.2025.2215

This work is licensed under a Creative Commons Attribution-NonCommercial 4.0 International License (CC BY-NC 4.0).

INTRODUCTION

Methane (CH₄) oversaturation in oxygenated (oxic) freshwater aquatic environments remains a key area of research that can have several impacts on the ecosystems. CH₄ is a potent greenhouse gas, and its production in oxic surface waters is not yet well understood. This «methane paradox» contradicts the traditional paradigm that CH₄ is exclusively produced under anoxic conditions and highlights the complexity of CH₄ cycling in freshwater systems (Grossart *et al.*, 2011; Bižić, 2021; Xun *et al.*, 2025). Freshwater ecosystems, such as lakes, rivers, and reservoirs, are major sources of atmospheric CH₄, contributing approximately 20% of global emissions (Saunois *et al.*, 2020). However, Laurentian Great Lakes remain underrepresented in global CH₄ budgets, creating a critical knowledge gap. This study focuses on Georgian Bay's embayment (Lake Huron) to address this gap and provide insights into biogeochemical CH₄ dynamics in the water column.

CH₄ production in oxic waters is driven by a combination of biological, chemical, and physical processes. Recent studies have identified multiple pathways for oxic CH₄ production (OMP), including the decomposition of organic matter (Repeta et al., 2016), the activity of methane-producing microbes (Grossart et al., 2011), photosynthetic activity (Bižić, 2021; Günthel et al., 2020; Ordonez et al., 2023), role of submerged macrophytes (Hilt et al., 2022), and the influx of CH₄ from sediments (Tang et al., 2014). Several phytoplankton groups produce CH₄ under oxic conditions, including diatoms, green algae, cryptophytes (Hartmann et al., 2020), and cyanobacteria (Bižić et al., 2020; Günthel et al., 2020), with light and temperature playing key regulatory roles (Yao et al., 2016; Klintzsch et al., 2020). Additionally, phosphorus limitation has been identified as a significant driver of OMP, with studies demonstrating that low soluble reactive phosphorus (SRP) concentrations enhance CH₄ production in oligotrophic systems including the metabolism of methylphosphonate (MPn) and other





organic compounds (Yao et al., 2016; Wang et al., 2021; Patel et al., 2024). Despite significant progress in understanding OMP, the mechanisms driving CH₄ accumulation and emissions in oxic waters remain debated (León-Palmero et al., 2020). Field and laboratory studies have revealed that CH₄ concentrations in the oxic layers of freshwater ecosystems can exceed those in marine environments, with multiple mechanisms contributing to CH₄ oversaturation (Grossart et al., 2011; Repeta et al., 2016; Tang et al., 2016). These mechanisms include lateral transport from littoral zones (Fernández et al., 2016), direct production in oxic waters (Bogard et al., 2014; Donis et al., 2017; Bižić, 2021), and ebullition from sediments (DelSontro et al., 2018; Donis et al., 2017). These studies highlight the need for integrated approaches to unravel the complex mechanisms driving CH₄ dynamics in freshwater systems.

In contrast to oxic CH₄ production, methanotrophy refers to the oxidation of methane and is a well-studied process carried out by methanotrophic microbes in freshwater lake sediments and anoxic water columns (Bastviken *et al.*, 2008; Borrel *et al.*, 2011). CH₄ can be oxidized by aerobic methanotrophs, particularly near the oxic-anoxic interface (Bastviken *et al.*, 2004, 2008; Borrel *et al.*, 2011). In fully anoxic and sulfate poor waters, anaerobic oxidation of methane (AOM) can occur via alternative electron acceptors such as iron (III), manganese (IV), nitrate, and nitrite (Egger *et al.*, 2015; Sivan *et al.*, 2011; Aromokeye *et al.*, 2020; He *et al.*, 2019). These processes play a significant role in mitigating CH₄ emissions, but their efficiency can vary depending on environmental conditions and microbial community composition (Su *et al.*, 2022).

Georgian Bay's embayment provides an ideal setting for studying CH₄ dynamics in surface waters. Its large surface area, complex shoreline morphology, and varying nutrient conditions create distinct biogeochemical gradients that influence CH₄ production and transport (Verschoor et al., 2017; Zastepa et al., 2021). The sheltered nature of embayments like North Bay of Honey Harbour goes through seasonal thermal stratification, is characterized by low sulfur and phosphorus concentrations, but high iron concentrations, creating a unique environment for microbial activity and studies of methane dynamics in this oligotrophic freshwater system. Therefore, the goal of this research was to analyze the CH₄ dynamics in the Georgian Bay embayment of Honey Harbour. We address key questions: How do CH₄ concentrations vary spatially and temporally, what are the primary drivers of methane production and accumulation in surface oxic waters and how do microbial communities influence methane dynamics. Additionally, we examine the role of redox-sensitive elements in CH₄ production and oxidation. This research advances our understanding of dynamics of CH₄ cycling in the Georgian

Bay's embayment and contributes to filling critical gaps in the CH₄ budget of the Laurentian Great Lake Huron.

METHODS

Site description and characteristics

Georgian Bay, forming the eastern extension of Lake Huron, stands as the biggest bay within the Laurentian Great Lakes (Fig. 1a). It reaches a maximum depth of 165m and covers a surface area of 15,108 km² (Lewis et al., 2008; McCarthy and McAndrews, 2012; Campbell and Chow-Fraser, 2017). Georgian Bay is located within the Great Lakes -St. Lawrence Forest Section in Canada, which extends from the sedimentary rock of the Bruce Peninsula in the south to the Sudbury- North Bay Forest zone in the north (Rowe, 1972). The Georgian Bay Formation, located within the Precambrian Shield, is composed out of thermally immature to mature gray shale and bioclastic-rich limestone beds (McIntosh et al., 2014). This bedrock has undergone weathering processes, leading to a coastline with the diverse structure of numerous embayments (McCarthy and McAndrews, 2012). The North Bay of Honey Harbour, an oligotrophic freshwater embayment of eastern Georgian Bay. The sampled Georgian Bay embayment is shallow with a maximum depth of ~17m (Fig. 1c) and is thermally stratified during summer. It is located between latitude 44°53′10″N and longitude 79°48′50″W. This embayment is a coastal system that is connected to Georgian Bay through narrow channels.

Overall, seasonal variations were indicated in both temperature levels and dissolved oxygen (DO) levels, with a trend of decreasing temperatures and increasing DO concentrations as the year progresses from summer to autumn (Tab. 1). The stratification occurred during the months of August and September, and water columns experienced hypoxic conditions during the stratification period.

Sampling

The samples were collected from the water column in the North Bay of Honey Harbour at the beginning of stratification, during the period of stable stratification, and at the end of stratification. Sampling location and depths by bathymetric map are shown in Fig. 1c. Samples were collected with the Georgian Bay Forever R/V using a multiparameter probe (YSI-Xylem Analytics, Yellow Springs Instruments, OH, USA) for measurements of physical and chemical parameters such as depth, temperature (°C), pH, ORP (mV), conductivity (μ S cm⁻¹), turbidity (NTU), salinity (PSU), dissolved oxygen (DO, mg L⁻¹), and dissolved oxygen saturation (%).

Tab. 1. Depth-integrated inventory of sampling site location, sampling depths, temperature, and the dissolved oxygen at the North Bay of Honey Harbour in Georgian Bay, Lake Huron (data for surface area and volume are from Campbell SD, Chow-Fraser P. 2017. Lake Huron, J Great Lakes Res 43:274-283).

Sampling date	Location	Surface area (km²)	Watershed area (km²)	Max depth (m)	Mean T (°C)	Max T (°C)	Mean DO (mg L ⁻¹)	Max DO (mg L ⁻¹)
19.07.2021	Latitude	1.886	9.180	16	17.6	23.6	5.3	9.4
23.08.2021	44°53′10″N			16	18.9	27.1	2.6	8.9
09.09.2021	longitude			17	17.8	21.6	3.7	7.8
19.10.2021	79°48′50″W			17	15.9	16.3	6.4	8.2

T, temperature; DO, dissolved oxygen.

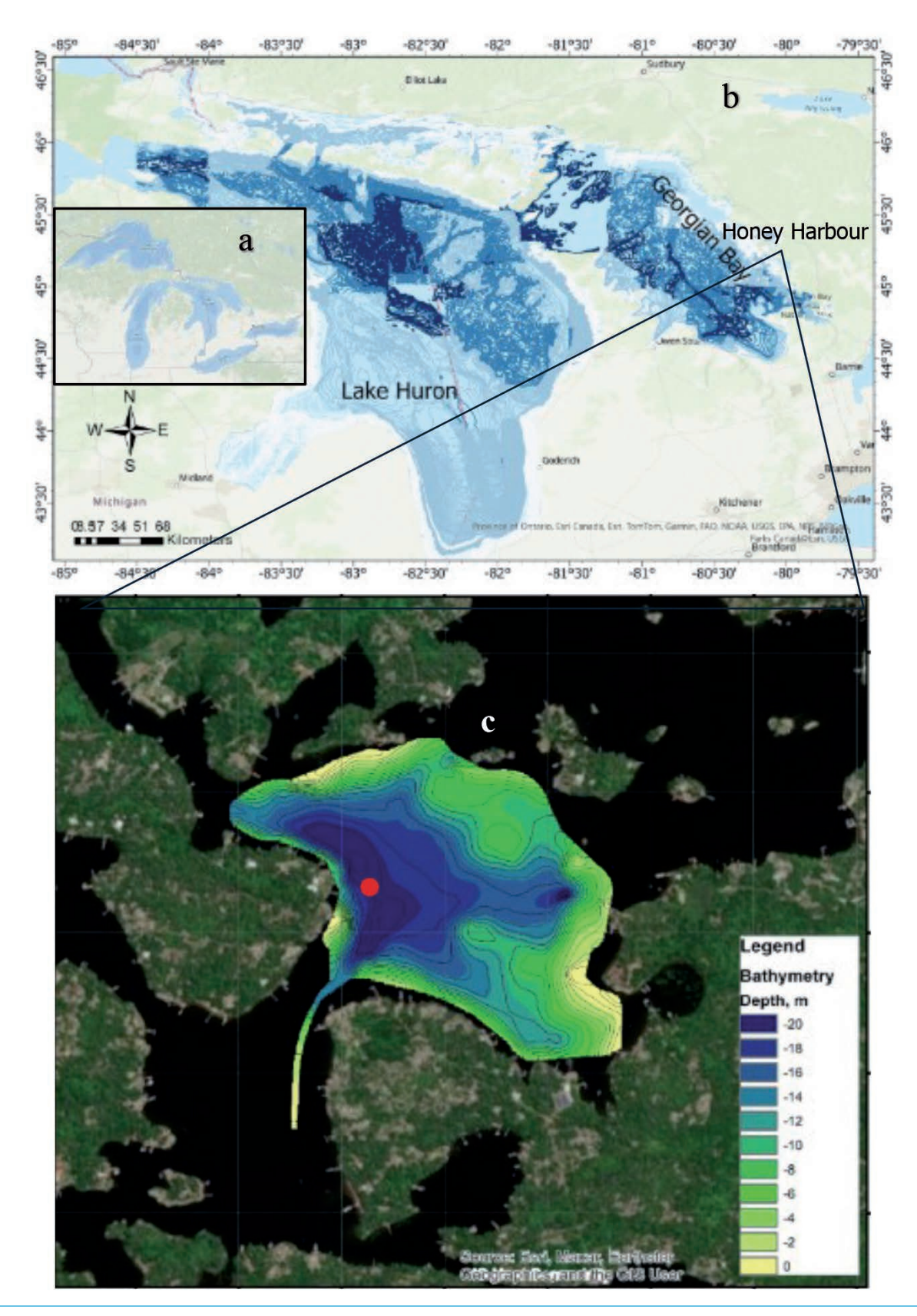


Fig. 1. Maps of the Laurentian Great Lakes (a) and Lake Huron with Georgian Bay (b). Sampling location with the bathymetric map of the North Bay of Honey Harbour (c).

Sensor calibrations were performed in the laboratory immediately prior to each field campaign following the protocols. The DO sensor was calibrated using a two-point calibration with airsaturated water and zero-oxygen solution. Instrument accuracy specifications for DO are ± 0.1 mg L^{-1} or $\pm 1\%$ of the reading, with a resolution of 0.01 mg L^{-1} . The pH, ORP, turbidity and conductivity sensors were calibrated using standard buffers and conductivity solutions, respectively. Temperature and depth sensors were factory-calibrated and checked for consistency during pre-deployment testing.

Before each deployment, the sonde was allowed to run in the lake for at least 20 min to equilibrate with the water temperature and stabilize the DO readings. All water samples were collected duplicate from near the surface to the bottom using a 5L Niskin bottle (General Oceanics Inc., Miami, FL, USA). During stratification periods, samples were collected from the metalimnion, epilimnion, and hypolimnion based on the thermocline readings from YSI. The samples for chemical composition and microbiological analysis were preserved immediately on board. Preservations of samples for analyses of nitrate, nitrite, ammonia, and phosphate were performed by freezing at -20°C. For measurements of total iron and manganese concentrations, water samples were preserved in the field in 5% (v/v) HNO₃ and stored at 4°C. Samples for DNA were filtered (1 L of water for each sample) through 0.2 µm nylon filters back in the laboratory and frozen at -20°C until extraction.

Underwater PAR (photosynthetically active radiation) irradiance was measured at the water subsurface and 1m intervals with a spherical quantum sensor (LI-192; LI-COR Biosciences, NE, USA). Measurements were corrected for variance in incident irradiance using a LI-190R quantum sensor (LI-COR Biosciences, NE, USA), which was attached to the lowering frame.

Water samples for CH₄ and CO₂ gas samples were collected using a 5L Niskin bottle and were quickly (max 5 min) transferred to pre-weighed serum bottles that were sealed with a butyl rubber stopper and crimped. Samples were kept at 4°C temperature until measurements. Instrument background was routinely monitored by running zero air on the Picarro G2132-i CRDS (Picarro Inc., USA) before and during each analytical session. These zero air measurements confirmed that background CH₄ and CO₂ levels remained below detection limits throughout the analysis period. The water samples for total alkalinity were preserved with a 1:10 ratio of saturated HgCl₂ solution. Water column samples were filtered through sterile 0.2 µm PES membrane filters (47 mm Supor 200, Pall, MI, USA) using a water pump; rolled up using sterile forceps; and transferred into sterile centrifuge tubes. The tubes with membrane filters were stored at -20°C until DNA extraction.

Analytical methods

Dissolved methane (CH₄), carbon dioxide (CO₂), and ¹³C-CO₂ isotopic composition were measured by cavity ring-down spectroscopy (CRDS) Picarro G2132-i analyser in duplicates. At each point, duplicate samples for CH₄ and CO₂ measurements were analysed using the headspace method. In the laboratory, headspace samples were retrieved using a gas-tight syringe and injected into the Picarro high-precision concentration and isotopic analyser. The concentrations and ¹³C-CO₂ isotopic composition from the headspace of the serum bottles were measured by CRDS Picarro G2132-i analyzer. Instrument-specific preci-

sion at ambient concentrations (1- σ of 5 min average) is δ^{13} C in CO_2 at $>0.1^{\circ}/_{00}$ precision, for [$^{12}CO_2$] is 200 range + 0.05% of reading and for $[^{12}CH_4]$ is 5 ppb + 0.05% of reading. The CH_4 and CO₂ concentration values were back-calculated accounting for the resulting headspace to water ratio in the bottle according to Henry's law constant calculated using solubility data provided by (Wilhelm et al., 1977). Samples of filters were extracted for chlorophyll using 90% aqueous acetone (v/v) as solvent (Schagerl and Künzl, 2007). Samples were disrupted and homogenized using vortex (5 s) then sonication in ice bath (Qsonica Q125 probe sonicator with probe diameter of 0.32 cm, for 20 s on a pulse mode (1 s on 1 s off) at 50 W), followed by 12 hours incubation at 4 °C in dark then centrifuged (×12000 g, 10 min) to remove particles and filter debris prior to measurements of Chl a concentrations. The Chl a concentrations were determined fluorometrically at an excitation wavelength of 430 nm and an emission wavelength of 663 nm (APHA, 1998).

For sulfate measurements, the samples were filtered through a 0.2 µm nylon filter and concentrations were measured by ion chromatography (IC; Metrohm 930 Compact IC) with a suppressor and a sodium carbonate/bicarbonate buffer as an eluent. The minimum detection limit (MDL) for this method is 1 µM. Iron concentrations were measured using SpectraMax 340PC microplate spectrophotometer. After the reduction of iron (III) with ascorbic acid and the treatment of the sample with Ferrozine reagent (Viollier et al., 2000). Dissolved manganese was detected using Genesys 10S UV-VIS (Thermo Scientific) spectrophotometric technique (Goto et al., 1977). Ascorbic acid was used to reduce total manganese to dissolved Mn2+. The sum of nitrate and nitrite concentrations was measured by the Griess method after the enzymatic reduction of nitrate to nitrite (Nims et al., 1995). Cayman Chemical 780001 kit was used for analyses. For ammonium determination, the indophenol method according to Krom (1980) was used. The soluble reactive phosphorus (SRP) was analysed based on the molybdenum blue method (Murphy and Riley, 1962). The total organic carbon (TOC) in the water column was measured by a Shimadzu TOC-VCPH/CPN (Shimadzu Model TOC-5000) based on the principle of oxidative combustion infrared (IR) analysis. The carbon samples were combusted to form $CO_{2(g)}$ and analysed in a nondestructive infrared analyzer (NDIR). The detection limit of quantification (LOQ) for TOC was around 500 ppb. In the laboratory, the total alkalinity was determined via Gran titration using a Metrohm 905 Titrando (Metrohm, Switzerland) (Stumm and Morgan, 1995).

Calculation of the CH₄ and CO₂ concentrations

The total gas concentration (TC) in the original water sample is calculated by determining the gas concentration of the headspace, converting this to the partial pressure of the gas, and then using this partial pressure to calculate the aqueous gas concentration that partitioned into the gas phase (C_{AH}), and the aqueous phase concentration that remained in the aqueous phase (C_{A}). The total concentration (TC) in the aqueous phase is then calculated by equation 1:

$$TC = C_{AH} + C_A (Eq. 1)$$

where: TC, total concentration of gas in the original aqueous sam-

ple; C_{AH} , aqueous gas concentration in the headspace after equilibrium; C_A , aqueous gas concentration in the water after equilibrium. The total concentration in the aqueous phase is then the sum of gas and aqueous phases by equation 2:

$$TC = \left(55.5 \frac{mol}{L}\right) * \frac{P_g}{H} * MW \left(\frac{g}{mol}\right) * 103 \left(\frac{mg}{g}\right) + \left[\left(\frac{V_h}{V_b - V_h}\right] * C_g * \left(\frac{MW \left(\frac{g}{mol}\right)}{22.4 \left(\frac{L}{mol}\right)}\right) * \left[\frac{273K}{T + 273K}\right] * 10^3 \left(\frac{mg}{g}\right)$$
(Eq. 2)

where the molar concentration of water (n_a/V) is assumed to be 55.5 mol L⁻¹ (molarity of pure water at 25°C, used for scaling aqueous concentrations), and MW is the molecular weight of the gas (g mol⁻¹). Here, n_a refers to the number of moles of water and V is the total aqueous volume in liters. The partial pressure of the target gas (Pg) in the headspace is calculated from the measured volumetric gas concentration (Cg in ppm), converted to a mole fraction by multiplying by 10⁻⁶. Henry's law constant (H) was applied (temperature corrected as described below) to calculate aqueous gas solubility. The volume of the aqueous phase (V_a) was determined as the difference between the bottle volume (V_b) and the headspace volume (V_h). The aqueous phase concentration (C_A) and the concentration of gas that partitioned into the headspace (C_{AH}) were then calculated and summed to determine the total dissolved gas concentration (TC). Gas density at standard temperature was used to convert volumetric concentrations to mass-based units, yielding results in milligrams of gas per liter of water (mg L⁻¹). Temperature-corrected values of Henry's law constant were calculated using solubility data provided by Wilhelm et al. (1977) and equation 3:

$$H = 1/\left[\exp\left\{\frac{A + \frac{B}{T} + C\ln\left(\frac{T}{K}\right) + DT}{R}\right\}\right]$$
 (Eq. 3)

Where, A, B, C, and D, are coefficients for gaseous solubility calculation (Wilhelm *et al.*, 1977; EPA method RSKSOP-175).

Mass balance calculations

To estimate the net production and consumption rates of methane ($\mathrm{CH_4}$) in the water column, we applied a mass balance approach using depth profile $\mathrm{CH_4}$ concentrations. The calculations were conducted for the period between August and September 2021 during stable stratification conditions. The study site is a semi-enclosed embayment with minimal riverine inflow, which *implies* limited external seeding of microbes. Given the stable stratification and lack of major inflows during this period, we assumed that concentration changes primarily reflected net biogeochemical processes (production and oxidation) within each depth layer. The net flux of methane ($\mathrm{F_{depths}}$) was determined using the following equation 4:

$$F_{depths} = \frac{(C_{date2} - C_{date1}) * V}{A*(date2 - date1)}$$
 (Eq. 4)

where, F_{depths} is the net methane flux (mg CH₄ m⁻² day⁻¹), C_{date2} and C_{date1} are measured CH₄ concentrations (mg L⁻¹) at two time points (August and September 2021), V is the volume of the water column segment (m³) calculated using bathymetric maps in Ar-

cGIS, A is the surface area corresponding to each depth interval (m²), and (date2 - date1) represents the time interval between measurements (days). The calculated flux values were converted to nM L⁻¹ d⁻¹ for visualization. Bathymetric contour maps were used to determine lake area and volume at each depth interval. Methane concentration data were measured from depth profiles collected during field sampling campaigns. The water column was divided into three distinct layers based on temperature stratification: Epilimnion (0-6 m), characterized by net methane production; Metalimnion (6-8 m), a transition zone where production declines; and Hypolimnion (8-16 m), predominantly showing methane consumption. Flux values were analyzed across these layers to assess spatial variability in methane production and oxidation. Net methane production (Pnet) was determined for each depth layer using the calculated fluxes, where positive values indicate methane production and negative values signify methane oxidation (equation 5):

$$P_{net} = \frac{(F_{depth2} - F_{depth1})}{dZ}$$
 (Eq. 5)

where P_{net} (nmol CH_4 L^{-1} d^{-1}) is the net methane production or consumption rate, F_{depth2} and F_{depth1} (nmol CH_4 m^{-2} d^{-1}) are the methane fluxes at two consecutive depth layers, and dZ (m) is the vertical distance between depth layers.

DNA extraction and analysis

The DNA extraction was conducted on filtered (1L) samples using PowerWater DNA Isolation Kit (QIAGEN, Hilden, Germany) per the manufacturer's instructions. Bacterial and archaeal 16S rRNA genes were amplified from DNA extracts from selected samples. DNA filters were stored at -20°C until sequenced. After extraction, purified amplicons were sent to MR DNA (http://www.mrdnalab.com, Molecular Research LP, Shallowater, TX, United States) for sequencing on an Illumina MiSeq (2 × 300 bp) sequencing platform. The 16S rRNA gene amplicon sequencing targeted the V4 variable region using the combined bacterial and archaeal primer set of 341F (CCTACGGGNGGCWGCAG) and 785R (GACTACHVGGGTATCTAATCC) (Klindworth et al., 2013). The forward and reverse sequences were joined, <150 base pair sequences and ambiguous base calls removed, and sequences were quality-filtered using error threshold 1.0. The dereplicated or unique sequences are denoised; unique sequences identified with sequencing or PCR point errors are removed, followed by chimera removal, thereby providing a denoised sequence. Final taxonomies were classified using BLASTn against a curated database derived from NCBI (www.ncbi.nlm.nih.gov). Phylum- and genus-level OTUs for bacteria and archaea with >4% abundance was reported.

Statistical analysis

Redundancy analysis (RDA) with the RStudio was used to determine statistically significant relationships between the microbial community composition of Archaeal and Bacterial Genus with environmental variables (concentrations of total iron (Fe), dissolved manganese (Mn), sulfate, dissolved oxygen (DO), methane (CH₄), temperature (T, $^{\circ}$ C), pH, PAR and ORP). Data was collected at different depths over the months of July, August, September, and October.

RESULTS

Physiochemical profiles

During July, dissolved oxygen (DO) concentrations dropped from 9.42 to 9.09 mg L^{-1} in the surface waters and were under 4 mg L^{-1} below the 15 m depth (Fig. 2a). During the stratification period, DO concentrations showed a sharp gradient between 7-9 m depth, and oxygen depletion was observed below depths of 7 m in August and 9 m in September (Fig. 2a). The water column in August could be divided into the oxic epilimnion (~1-6 m; DO=6.39-8.94 mg L^{-1} ; Fig. 2a) and anoxic bottom waters (~7-16 m; DO<4 mg L^{-1} ; Fig. 2a). In September, the water column DO at the surface (~1-9 m) ranged from 4.85–7.8 mg L^{-1} , while in the anoxic bottom (~10-16 m), it was below 4 mg L^{-1} (Fig. 2a).

Temperature profiles show thermal stratification across months, with surface temperatures starting at around 24°C in July and changing to approximately 16.5°C by October (Fig. 2b). A stable thermal gradient was observed, indicating the persistence of a thermocline throughout the summer-autumn season (Fig. 2b). The temperature profiles showed a mixed water mass occupying the upper parts of the water column during July and October (Fig. 2b). While the water column was stratified during two samplings in August and September, the thermocline was evidenced by gradients in temperature between 8-10 m and 7-11 m during August and September, respectively (Fig. 2b). High temperatures (T=22.5-27.1°C) in the oxic zone, mid-temperatures (T=18.5-21.5°C) in the sub-oxic zone, and low temperatures (T=11.8-16.1°C) in the anoxic zone were measured (Fig. 2b). The surface waters had temperatures of 21.4-21.6°C in the oxic zone, and 12.6-15.5°C in the anoxic zone (Fig. 2b). The water column temperature from surface to bottom waters ranged from 9.9°C to 23.6°C in July and 14.5°C to 16.3°C in October (Fig. 2b).

Oxidation-reduction potential (ORP) profiles showed strong vertical gradients. Surface ORP values peaked at 319.8 mV in July, declining to -38.9 mV at 16 m (Fig. 2c). In August and September, ORP gradients intensified near the chemocline (Fig. 2c), while by October, values stabilized across the water column due to mixing (Fig. 2c). The pH ranged from 6.48 in July to 7.59 in October, with surface waters transitioning from mildly acidic to slightly basic conditions (Fig. 2d). Conductivity values ranged from 130 to $145~\mu S$ cm $^{-1}$, peaking in August and remaining stable through October (Fig. 2e).

The chlorophyll a (Chl a) concentrations showed distinct vertical and temporal variations from July to October 2021 (Fig. 2f). In July, the highest Chl a were observed at 8 m (7.12 μ g L⁻¹) and 7 m (6.35 μ g L⁻¹), with moderate levels at 1 m (2.34 μ g L⁻¹) and lower concentrations at 16 m (0.860 μ g L⁻¹). August had a significant increase in Chl a at 6 m (12.83 μ g L⁻¹) and 5 m (11.06 μ g L⁻¹). In September, the peak Chl a concentration was at 8 m (8.205 μ g L⁻¹), with lower values at 2 m (1.084 μ g L⁻¹) and 16 m (0.175 μ g L⁻¹). By October, Chl a generally decreased, with the highest concentration at 11 m (2.837 μ g L⁻¹) and the lowest at 2 m (0.210 μ g L⁻¹) (Fig. 2f).

 CH_4 concentrations peaked repeatedly at the chemocline and coincided with oxygen oversaturation and higher PAR values (Fig. 3 a-d). The CH_4 profile was consistent across the four samplings, with low concentrations in the hypolimnion and high concentrations in the chemocline and epilimnion. Surface CH_4 concentrations were $1.88\pm0.01~\mu g~L^{-1}$ at 1~m depth in July, $0.95\pm0.01~\mu g~L^{-1}$ at 1~m depth in August, $4.69\pm0.01~\mu g~L^{-1}$ at 2~m depth in September 1.88 $\pm0.01~\mu g~L^{-1}$ at 1~m depth in September 1.89 $\pm0.01~\mu g~L^{-1}$ at 1~m dept

tember, and $1.43\pm0.01~\mu g~L^{-1}$ in October at 1-2 m depths (Fig. 3 a-d). In July, CH₄ concentrations declined with depth until the chemocline, which persisted during stable stratification in August and September but eroded in October. Below the chemocline, CH₄ concentrations were lowest at $0.29\pm0.07~\mu g~L^{-1}$ in July, $0.28\pm0.01~\mu g~L^{-1}$ in August, $0.27\pm0.01~\mu g~L^{-1}$ in September, and $0.35\pm0.07~\mu g~L^{-1}$ in October at depths of 16-17 m (Fig. 3 a-d).

Iron and manganese profiles show redox sensitivity below the oxic-anoxic interface. Total iron (Fe_{tot}) concentrations peaked below the chemocline, ranging from 3.48±0.03 μM L $^{-1}$ in July to 24.3±0.38 μM L $^{-1}$ in September at 16 m (Fig. 3 a-c). Dissolved manganese (Mn $^{2+}$) concentrations were consistently higher than iron, peaking at 2.02±0.03 μM L $^{-1}$ in August and 34.62±0.25 μM L $^{-1}$ in October (Fig. 3 a-d). High Mn $^{2+}$ levels in the hypolimnion highlight reducing conditions.

Photosynthetically active radiation (PAR) profiles showed rapid attenuation with depth. In July, PAR values declined from 2396 μ M photons s⁻¹ m⁻² at 1 m to 5.73 μ M photons s⁻¹ m⁻² at 7 m (Fig. 3a). Similar patterns were observed in August and September (Fig. 3 b,c). By October, PAR penetration remained limited to surface layers, with values diminishing to less than 0.5 μ M photons s⁻¹ m⁻² below the chemocline (Fig. 3d).

Sulfate concentrations in surface waters ranged from 51.34 to 55.38 μ M L⁻¹, decreasing steadily with depth across all months (Fig. 4 a-d). Ammonium (NH₄⁺) concentrations peaked at 1.67±0.3 μ M L⁻¹ in July at 7 m and 3.1±0.43 μ M L⁻¹ in August at 8 m, with reduced values observed in September and October. Nitrate (NO₃⁻) concentrations were highest in August at 5.39±0.06 μ M L⁻¹ at 7 m and declined in subsequent months. Soluble reactive phosphorus (SRP) showed concentrations of 0.71±0.16 μ M L⁻¹ in July and 1.44±0.07 μ M L⁻¹ in August (Fig. 4 a-d).

Total organic carbon (TOC) concentrations peaked in surface waters at 4.47 ± 0.02 mg L⁻¹ in July and declined to 3.50 ± 0.07 mg L⁻¹ at depth (Fig. 5a). Dissolved CO₂ concentrations were higher in the hypolimnion, with maximum values of 7.25 ± 0.37 mg L⁻¹ in August at 16 m and minimum values of 1.51 ± 0.31 mg L⁻¹ in October (Fig. 5 a-d). The δ^{13} C-CO₂ values ranged from $-15.9\pm0.005\%$ in July to $-21.2\pm0.006\%$ in September. The relationship between CH₄, CO₂, and δ^{13} C-CO₂ indicates active carbon cycling driven by redox gradients and seasonal stratification.

Potential production and consumption of CH₄ (August-September)

The calculated net CH₄ production rate (P_{net}) (Fig. 6), varied at different depths between months of stable stratification period. At the shallowest depth of 1 m, the production is 6.86 nM·L⁻¹d⁻¹, indicating a high rate of CH₄ production. The highest net production rate from August to September was at 7.22 nM·L⁻¹d⁻¹ at 2m. As the depth increases to 5 m and 6 m, the CH₄ production rates decrease to 2.11 and 0.23 nM·L⁻¹d⁻¹, respectively. CH₄ net production ranged between 6.85 and 0.22 nM·L⁻¹d⁻¹ in the surface oxic waters between depths of 1-6 m (Fig. 6). The CH₄ production rates in the top 5 m during the stable stratification months are much greater than those in the metalimnion (Figs. 3 b,c and Fig. 6). From a depth of 7 m downwards, the flux values reveal a shift to CH₄ consumption. The net consumption rates were estimated to be between -1.29 to -1.47 nM·L⁻¹d⁻¹ between depths of 7-10 m, indicating that CH₄ consumption in observed hypolimnion water depths between August and September was on the rise, and CH₄ oxidation was occurring below the chemocline. The consumption rate at the deepest point of 16 m was -0.95 nM·L⁻¹d⁻¹ (Fig. 6).

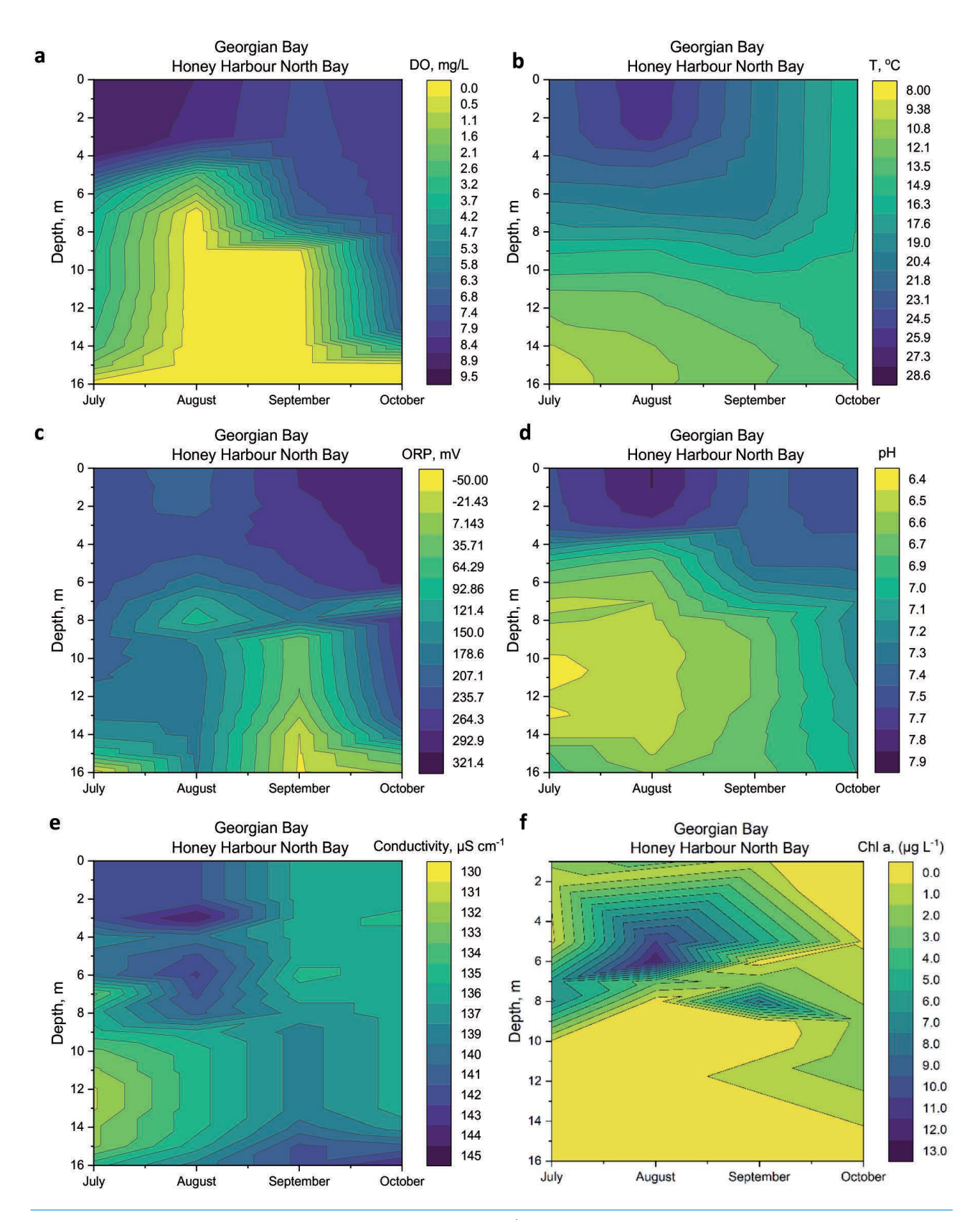


Fig. 2. Contour plots of depth profiles. a) Dissolved oxygen (DO-mg L^{-1}). b) temperature (T, °C). c) Oxidation-reduction potential (ORP, mV). d) pH. e) Conductivity (μ S cm⁻¹). f) Chl a (μ g L^{-1}).

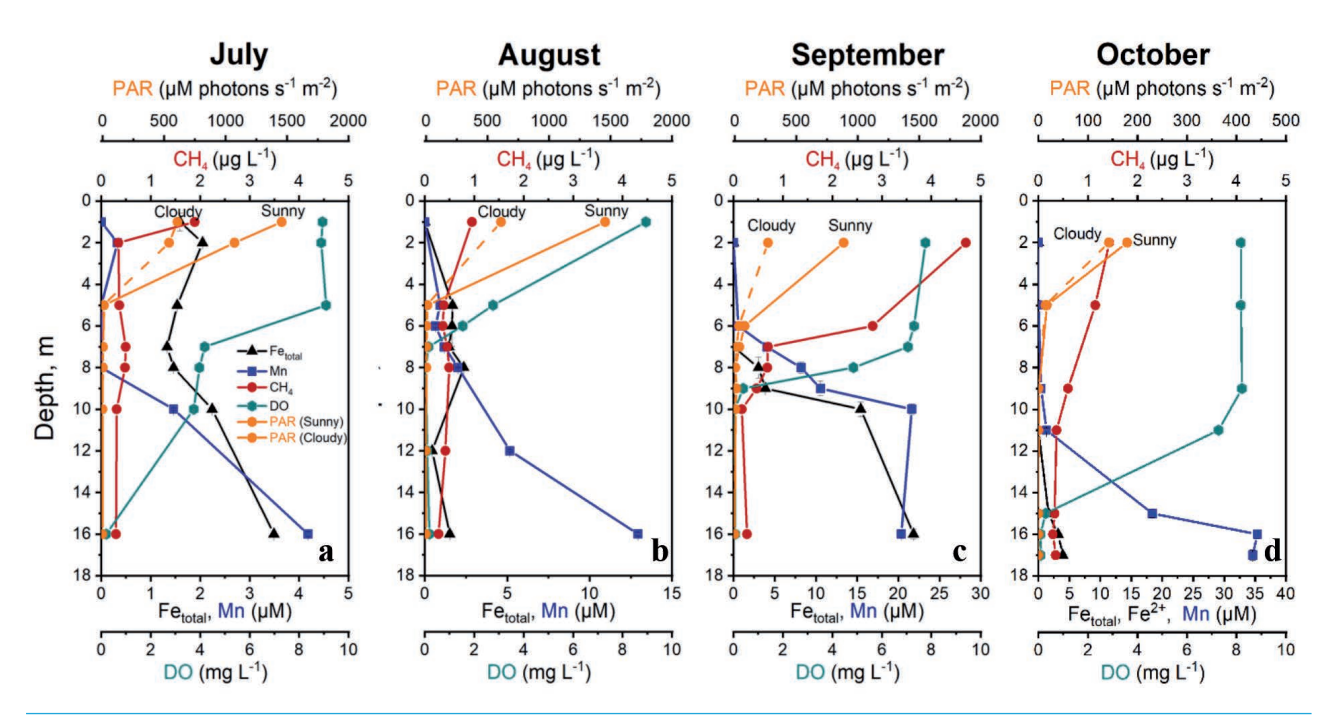


Fig. 3. Seasonal depth profiles of environmental variables in the water column from July to October. a-d) Data for each month. Methane concentrations (CH₄, μ g L⁻¹), dissolved oxygen (DO, mg L⁻¹), photosynthetically active radiation (PAR, μ M photons s⁻¹ m⁻²; sunny and cloudy conditions), and dissolved metals (Fe_{total}, μ M L⁻¹; Mn, μ M L⁻¹) are shown.

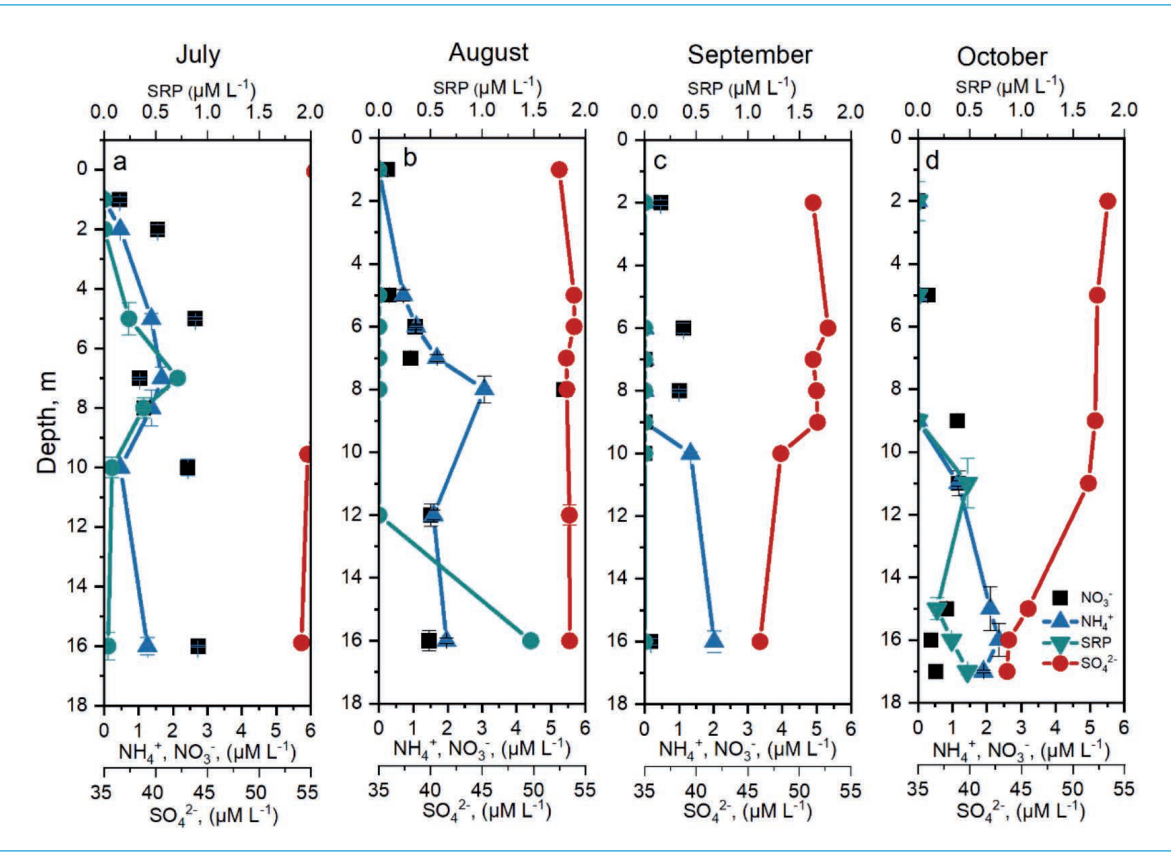


Fig. 4. Depth profiles of nutrients and sulfate concentrations in Honey Harbour North Bay across different months. a-d) Represent July, August, September, and October, respectively. Concentrations of ammonium (NH₄⁺, μM L⁻¹), nitrate (NO₃⁻, μM L⁻¹), sulfate (SO₄²⁻, μM L⁻¹), and soluble reactive phosphorus (SRP, μM L⁻¹) are shown.

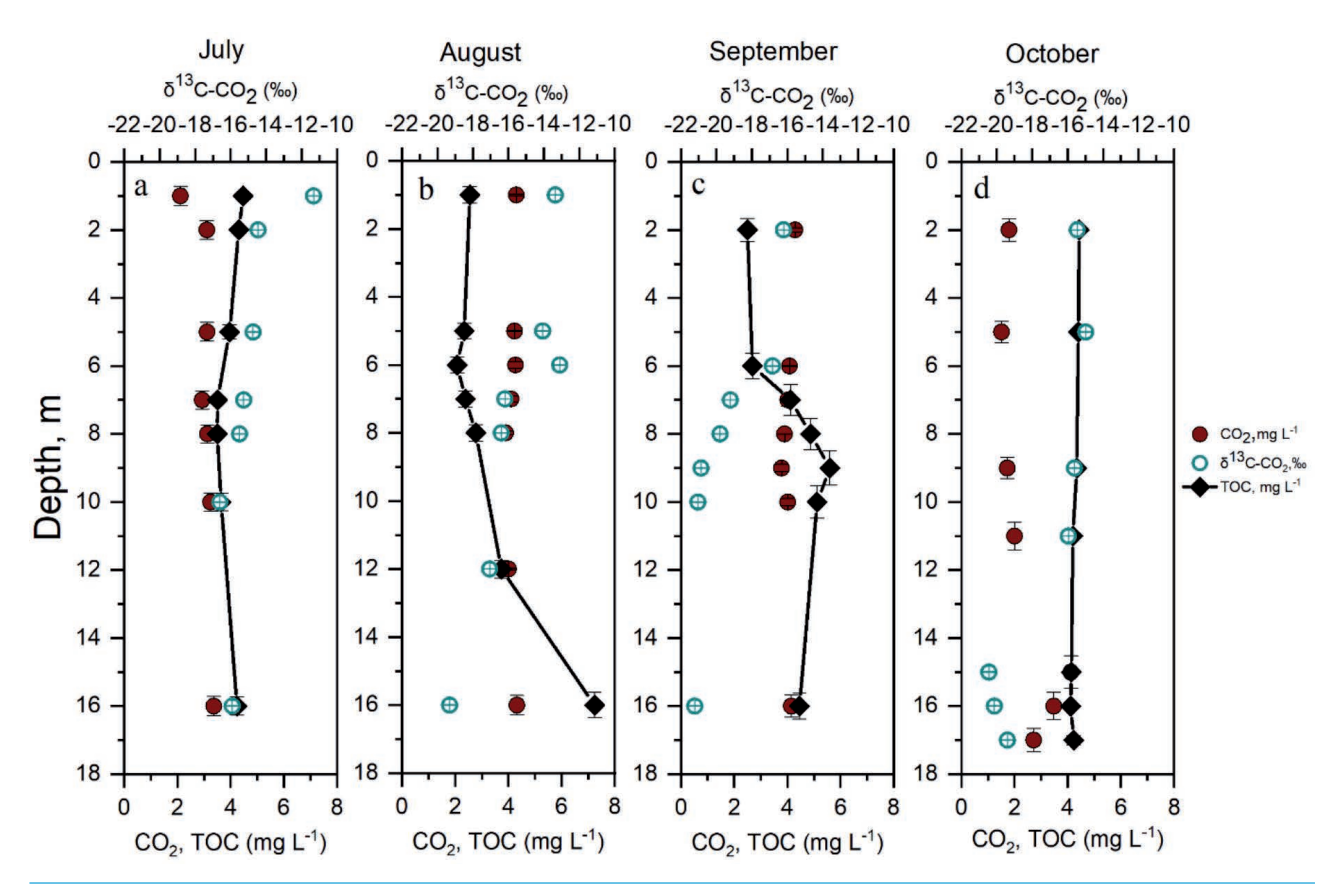


Fig. 5. Depth profiles of TOC and CO₂ concentrations, and δ^{13} C-CO₂ isotopes in Honey Harbour North Bay across July, August, September, and October (a-d). Panels show dissolved CO₂ concentrations (mg L⁻¹, red circles), total organic carbon (TOC, mg L⁻¹, black diamonds), and δ^{13} C-CO₂ values (‰, blue circles).

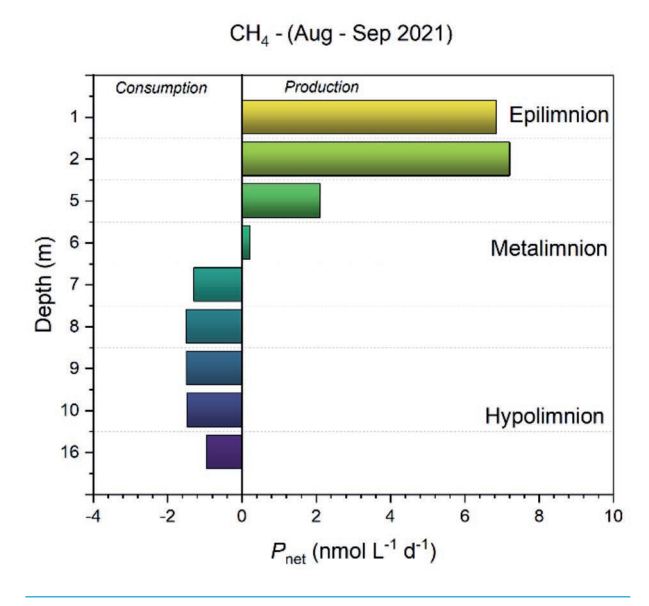


Fig. 6. Net CH_4 production and consumption rates (P_{net} , nmol L^{-1} d⁻¹) in Honey Harbour North Bay during the stratification period between the months of August and September 2021.

Microbial community composition

Microbial community composition displayed distinct temporal and depth-related variation over the stratification period (Fig. 7a). Proteobacteria, Actinobacteria, and Bacteroidetes were the dominant phyla across most samples, with additional but lower relative contributions from Verrucomicrobia, Eurvarchaeota, Cvanobacteria, Planctomycetes, Firmicutes, and Acidobacteria. July surface (1-5 m) and mid-depth (7-8 m and 10-16 m) samples were characterized by high relative abundances of Actinobacteria (up to 68%), and absence of Verrucomicrobia and Planctomycetes. In contrast, August and September samples exhibited increased Verrucomicrobia (up to 13%) and Planctomycetes (up to 12%), particularly in the epilimnion and metalimnion layers. Firmicutes represented the third most abundant phylum, with relative abundances ranging from 4.2% to 21.4%. The highest Firmicutes abundance was observed in July samples, particularly at 10-16 m depth (21.4%), suggesting depth-stratified community preferences. Bacteroidetes showed sporadic occurrence, being completely absent from several samples but reaching up to 6.8% in July surface waters. Euryarchaeota were detected primarily in August and September between 1-8 m, with relative abundances ranging from 2 to 4%, while Cyanobacteria appeared sporadically in early August and September (maximum 2.6%).

Venn diagram analysis showed monthly shifts in the number of phyla and geochemical parameters correlated with methane concentrations, with the highest overlap of methane-associated phyla and environmental variables occurring in September (Fig. 7b). August samples showed the highest number of methane-correlated phyla (8 total), suggesting peak activity of methane-related processes during this period. This coincided with intermediate temperatures and optimal conditions for both methanogenesis and methane oxidation. September samples displayed reduced methane-associated diversity (4 phyla), while October showed the most restricted community (3 phyla), indicating seasonal decline in methane cycling activity.

Redundancy analysis (RDA) at the Archaea and Bacteria genus level showed associations between certain genus and geochemical variables such as CH₄, redox potential, and dissolved oxygen, with separation between August and September samples along RDA1 and RDA2 axes. The ordination revealed that methane concentration (CH₄), dissolved oxygen (DO), and oxidation-reduction potential (ORP) were the primary environmental drivers structuring archaeal communities.

DISCUSSION

Methanogenesis in oxic waters

The detection of methanogenic archaea in oxygenated surface waters aligns with growing evidence from other freshwater and marine systems showing that methanogens can persist, and potentially remain active, under oxic conditions (Grossart et al., 2011; Donis et al., 2017; Günthel et al., 2019, 2020). This contributes to ongoing discussions about the microbial niches of methanogens in oxic environments. The seasonal variations in methanogen abundance suggest that environmental conditions such as temperature, nutrient availability, and organic matter input can influence methane production. Fig. 7a highlights the Eurvarchaeota at surface waters reaching around 3-4% at 1-6 m depths in August and September 2021. Our results indicate that Methanomicrobium and Methanobacterium were abundant in the epilimnion, reaching 55.6% and 16.7% at 1-5 m in July, 19% and 4.8% at 2-6 m in September and 5.3% at 2-5 m in October (Fig. 7d), suggesting that methane production occurs under oxic conditions (Fig. 7d).

However, both in oxic and anoxic waters, ammonia-oxidizing archaea may also contribute to CH₄ cycling. The presence of Candidatus Nitrosoarchaeum, which constituted 20% in August at 1m, 23.8% in September at 2-6m, and 94.7% at 2-5 m in October, indicates potential interactions between methane and nitrogen cycling, particularly ammonia oxidation, which has been linked to methane production in certain aquatic environments (Zhu et al., 2012). The presence of Candidatus Nitrosoarchaeum, an ammonia-oxidizing archaeon, at mid-depths (5-8 m in August and 2-15 m in October) further supports this interaction. Some aerobic bacteria (specifically, Acidovorax species) can produce methane under oxic conditions via the metabolism of methylated amines, which links nitrogen and carbon cycling in freshwater environments (Wang et al., 2021). The MPn degradation has been shown to produce methane as a byproduct in phosphorus-limited lakes, driven by bacterial C-P lyase activity (Yao et al., 2016; Wang et al., 2017).

Our results show that Methanomicrobium and Methanobac-

terium were abundant in the epilimnion, reaching 55.6% and 16.7% at 1-5 m in July, 19% and 4.8% at 2-6 m in September and 5.3% at 2-5 m in October (Fig. 7d), suggesting that methane production occurs under oxic conditions. Previous studies showing that certain methanogens can tolerate low oxygen concentrations and remain metabolically active (Yao et al., 2016). These methanogens are traditionally considered strictly anaerobic, but their persistence in oxic waters indicates either oxygen tolerance or localized anaerobic niches within particulate organic matter. This is consistent with studies demonstrating that methanogens can survive in oxygenated waters associating with other microbes that consume oxygen, creating micro-scale anoxic zones (Grossart et al., 2011; Donis et al., 2017). The detection of Methanosaeta in surface waters (40% at 1 m in August among Archaea) also supports that acetoclastic methanogenesis may be occurring in surface oxic waters during stratification within suspended organic particles (Mori et al., 2012).

The RDA results (Fig. 7d) highlight the strong positive correlation between methanogenic archaea and primary production, as evidenced by the clustering of *Methanomicrobium* and *Methanobacterium* near elevated CH₄ concentrations and photosynthetic activity. The RDA analysis suggests that methanogen abundance is positively correlated with high PAR and DO levels, which aligns with recent studies showing oxygen-tolerant methanogenic activity in lake epilimnia (Bižić *et al.*, 2020; Günthel *et al.*, 2020). These results align with studies from freshwater lakes and coastal systems where methane production has been attributed to MPn degradation by Cyanobacteria under phosphorus-limited conditions, a process that generates CH₄ in oxic waters (Repeta *et al.*, 2016; Bižić *et al.*, 2020).

Role of Cyanobacteria in CH₄ production

Cyanobacteria are key contributors to CH₄ production in oxygen-rich waters, particularly under phosphorus-limited conditions. During the study, *Synechococcus* were abundant in the epilimnion, with their peak abundance coinciding with elevated CH₄ concentrations in August and September (Fig. 7c). This spatial and temporal overlap supports that photoautotrophs play a direct role in CH₄ production, likely through the enzymatic breakdown of MPn (Repeta *et al.*, 2016). The low phosphorus availability in surface waters during the study period (Fig. 4) supports this mechanism, as phosphorus stress often triggers MPn utilization in aquatic systems (Beversdorf *et al.*, 2010).

Laboratory experiments have demonstrated that Cyanobacteria, including Synechococcus, can produce CH4 under oxic conditions, particularly under high light availability (Klintzsch et al., 2020; Bižić et al., 2020). This aligns with our observation that CH₄ concentrations correlated with PAR intensities (Fig. 4 a-d), suggesting that light-driven microbial metabolism contributes to CH₄ formation in surface waters. Additionally, Cyanobacteria-mediated CH₄ production may be linked to stress responses, such as oxidative stress, which can lead to the breakdown of methylated precursors (Lenhart et al., 2016). The possibility of micro-anoxic niches within phytoplankton aggregates providing localized anaerobic conditions for methanogenesis further complicates the traditional understanding of CH₄ production (Tang et al., 2016). The RDA results (Fig. 7c) describing the connection between CH₄ production and Cyanobacteria, Synechococcus closely associated with CH₄ concentrations and environmental variables such as PAR and SRP availability. Our

results align with previous studies demonstrating that Cyanobacteria contribute to CH₄ cycling in both freshwater systems through MPn degradation and light-driven metabolic pathways (Yao *et al.*, 2016; Bižić *et al.*, 2020).

CH₄ production and consumption dynamics

CH₄ concentrations in Honey Harbour's North Bay exhibit distinct spatial and seasonal trends, with the highest concentrations found in the oxic epilimnion (top 5 m) and declining with depth due to CH₄ oxidation. Net production and consumption rates indicate that CH₄ production in surface waters increased from August to September (Fig. 6), coinciding with periods of high Cyanobacterial abundance and photosynthetic activity. This suggests that the oxic epilimnion serves as the primary CH₄ production zone during stable stratification, while CH₄ oxidation dominates below the oxic-anoxic interface (Fig 7c).

During late summer stratification (August-September), surface CO_2 concentrations declined while CH_4 and TOC levels increased in the epilimnion. Although photosynthetic uptake may have contributed to the CO_2 drawdown, the concurrent shift toward more negative $\delta^{13}C$ - CO_2 values indicates input of isotopically light CO_2 , primarily from heterotrophic respiration. Minor contributions from methane oxidation are also possible where CH_4 and oxygen co-occur, but given the lower CH_4 concentrations, its overall influence on the $\delta^{13}C$ - CO_2 signal was likely limited. In the hypolimnion, both CO_2 concentrations and ^{13}C -depletion increased with depth, consistent with ongoing remineralization of organic matter below the chemocline.

This oxidation of methane below the chemocline is likely driven by aerobic methanotrophs, such as *Methylobacter* near the oxic-anoxic interface, and by Fe- and Mn-dependent anaerobic oxidation of methane (AOM) at greater depths.

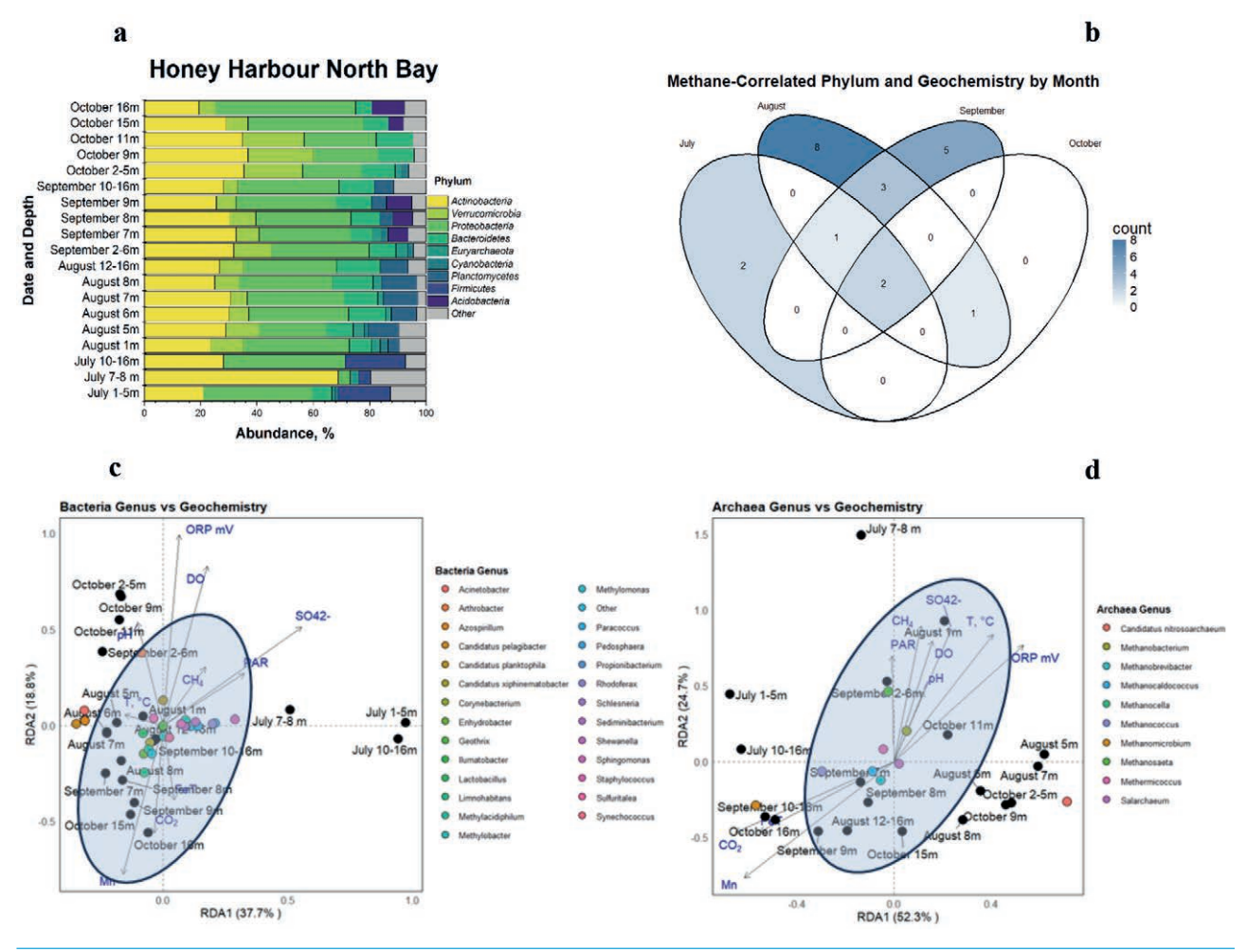


Fig. 7. Microbial community structure, diversity, and environmental correlations in the water column of Honey Harbour North Bay (Georgian Bay, Lake Huron) across sampling months in 2021. a) Relative abundance of dominant prokaryotic phyla across depths and sampling dates. b) Venn diagram illustrates the number of methane-associated phyla and geochemical parameters detected and in common across the four sampling months. c) Redundancy analysis (RDA) showing relationships between Bacteria genus community composition and measured geochemical parameters. d) Archaeal genus community composition and measured geochemical parameters. Sample points (black dots) denote individual depth and month combinations used in each ordination.

The increasing abundance of Fe- and Mn-reducing bacteria, such as *Geothrix* and *Shewanella*, below the chemocline (where CH₄ consumption is highest) indicates that metal-coupled CH₄ oxidation plays an important role in regulating CH₄ fluxes in the hypolimnion (Su *et al.*, 2022). This aligns with previous studies in stratified lakes and coastal systems, where metal oxides serve as electron acceptors in CH₄ oxidation pathways (Egger *et al.*, 2015; Sivan *et al.*, 2011; Su *et al.*, 2020). The correlation between CH₄ oxidation and Fe/Mn cycling in our study supports the role of metal-dependent microbial processes in controlling CH₄ dynamics, consistent with findings from Fe-rich lacustrine environments (Ettwig *et al.*, 2016; He *et al.*, 2019).

The interplay between methane-producing and CH_4 -consuming microbes regulates CH_4 dynamics in the embayment. If methanotrophic activity decreases due to environmental limitations (e.g., temperature, light, or nutrient availability), CH_4 may accumulate, increasing CH_4 flux to the atmosphere. Future studies should aim to quantify the relative contributions of microbial-driven CH_4 production and consumption pathways through incubation experiments, as well as their role in regulating CH_4 fluxes from sediments and emissions to the atmosphere.

CONCLUSIONS

This study provides compelling evidence that CH₄ production in the oxygenated surface waters of the Georgian Bay embayment is driven by microbial processes involving both methanogenic Archaea and Cyanobacteria. The presence of methanogens in the oxic epilimnion, their correlation with environmental factors such as PAR, DO, and temperature, and the dominance of Cyanobacteria suggest that CH₄ oversaturation results from a combination of photoautotrophic and archaeal methanogenesis. Additionally, the low phosphorus availability likely enhances CH₄ production through MPn degradation, a pathway extensively reported in oligotrophic freshwater systems. Below the oxic-anoxic interface, CH₄ oxidation is primarily mediated by Fe/Mn-dependent biogeochemical processes, leading to CH4 consumption at hypolimnion depths. These results challenge conventional views on methane production in oxic freshwaters and underscore the need for further research on alternative CH₄ production pathways in freshwater ecosystems. Despite these findings, uncertainties remain regarding the specific enzymatic mechanisms driving CH₄ production in oxic waters, highlighting the need for further research. Understanding the drivers of CH₄ production in oxygenated waters of Georgian Bay's embayments is important for improving CH₄ budget in Laurentian Great Lake Huron, particularly in response to climate-driven changes in freshwater aquatic ecosystems.

ACKNOWLEDGMENTS

The authors thank NSERC Discovery Grant RGPIN-06184 to M.D., Alex Neumann for help with mass balance calculations and bathymetric mapping, Carl Mitchell for providing multiparameter sonde, Zach DiLoreto for helping with the laboratory measurements, and Serra-Willow Buchanan, Ken Welch (UTSC), and Gregor Lucic (Picarro, Inc.) for providing access and assistance to Picarro Instruments with CH_4 and CO_2 analysis.

REFERENCES

- Aromokeye DA, Kulkarni AC, Elvert M, Wegener G, Henkel S, Coffinet S. 2020. Rates and microbial players of iron-driven anaerobic oxidation of methane in methanic marine sediments. Front Microbiol 10:3041
- APHA 1998. Standard Methods for the Examination of Water and Wastewater. 20th Edition, American Public Health Association, American Water Works Association and Water Environmental Federation, Washington DC.
- Bastviken D, Cole J, Pace M, Tranvik L. 2004. Methane emissions from lakes: Dependence of lake characteristics, two regional assessments, and a global estimate. Glob Biogeochem Cycles 18:1-12.
- Bastviken D, Cole JJ, Pace ML, Van de-Bogert MC. 2008. Fates of methane from different lake habitats: Connecting whole-lake budgets and CH4 emissions. J Geophys Res Biogeosci 113:G02024.
- Bastviken D, Tranvik LJ, Downing JA, Crill PM, Enrich-Prast A. 2011. Freshwater methane emissions offset the continental carbon sink. Science 331:50.
- Beversdorf LJ, White AE, Björkman K, Letelier RM, Karl DM. 2010. Phosphonate metabolism of Trichodesmium IMS101 and the production of methane in the upper ocean. Limnol Oceanogr 55:1768-1778.
- Bižić-Ionescu M, Ionescu D, Günthel M, Tang KW, Grossart HP. 2018. Oxic methane cycling: New evidence for methane formation in oxic lake water, pp. 1-22. In: Stams AJM, Sousa D (eds.), Biogenesis of hydrocarbons. Springer.
- Bižić M. 2021. Phytoplankton photosynthesis: An unexplored source of biogenic methane emission from oxic environments. J Plankton Res 43:822-830.
- Bižić M, Klintzsch T, Ionescu D, Hindiyeh MY, Günthel M, Muro-Pastor AM, et al. 2020. Aquatic and terrestrial cyanobacteria produce methane. Sci Adv 6:eaax5343.
- Bogard MJ, del Giorgio PA, Boutet L, Chaves MC, Prairie YT, Merante A, Derry AM, 2014. Oxic water column methanogenesis as a major component of aquatic CH₄ fluxes. Nat Commun 5:5350.
- Borrel G, Jézéquel D, Biderre-Petit C, Morel-Desrosiers N, Morel JP, Fonty G, Lehours AC. 2011. Production and consumption of methane in freshwater lake ecosystems. Res Microbiol 162:832-847.
- Campbell SD, Chow-Fraser P. 2017. Models to predict total phosphorus concentrations in coastal embayments of eastern Georgian Bay, Lake Huron. J Great Lakes Res 43:274-283.
- DelSontro T, del Giorgio PA, Prairie YT. 2018. No longer a paradox: The interaction between physical transport and biological processes explains the spatial distribution of surface water methane within and across lakes. Ecosystems 21:1073-1087.
- Donis D, Flury S, Stockli A, Spangenberg JE, Vachon D, McGinnis DF. 2017. Full-scale evaluation of methane production under oxic conditions in a mesotrophic lake. Nat Commun 8:1661.
- Egger M, Rasigraf O, Sapart CJ, Jilbert T, Jetten MSM, Röckmann T, et al. 2015. Iron-mediated anaerobic oxidation of methane in brackish coastal sediments. Environ Sci Technol 49:277-283.
- Ettwig KF, Zhu B, Speth D, Keltjens JT, Jetten MSM, Kartal B.

- 2016. Archaea catalyze iron-dependent anaerobic oxidation of methane. P Natl Acad Sci USA 113:12792-12796.
- Fernández E J, Peeters F, Hofmann H, 2016. On the methane paradox: Transport from shallow water zones rather than in situ methanogenesis is the major source of CH₄ in the open surface water of lakes. J Geophys Res Biogeosci 121:2717-2726.
- Goto K, Taguchi S, Fukue Y, Ohta K, Watanabe H. 1977. Spectrophotometric determination of manganese with 1-(2-pyridylazo)-2-naphthol and a non-ionic surfactant. Talanta 24: 752-753.
- Grossart HP, Frindte K, Dziallas C, Eckert W, Tang KW. 2011. Microbial methane production in the oxygenated water column of an oligotrophic lake. P Natl Acad Sci USA 108:19657-19661.
- Günthel M, Donis D, Kirillin G, Ionescu D, Bizic M, McGinnis DF, et al. 2019. Contribution of oxic methane production to surface methane emission in lakes and its global importance. Nat Commun 10:5497.
- Günthel M, Klawonn I, Woodhouse J, Bižić M, Ionescu D, Ganzert L, et al. 2020. Photosynthesis-driven methane production in oxic lake water as an important contributor to methane emission. Limnol Oceanogr 65:2853-2865.
- Hartmann JF, Günthel M, Klintzsch T, Kirillin G, Grossart HP, Keppler F. 2020. High spatiotemporal dynamics of methane production and emission in oxic surface water. Environ Sci Technol 54:1451-1463.
- He Q, Yu L, Li J, He D, Cai X, Zhou S. 2019. Electron shuttles enhance anaerobic oxidation of methane coupled to iron(III) reduction. Sci Total Environ 688:664-672.
- Hilt S, Grossart HP, McGinnis DF, Keppler F. 2022. Potential role of submerged macrophytes for oxic methane production in aquatic ecosystems. Limnol Oceanogr 67:S76-S88.
- Klindworth A, Pruesse E, Schweer T, Peplies J, Quast C, Horn M, Glöckner FO. 2013. Evaluation of general 16S ribosomal RNA gene PCR primers for classical and next-generation sequencing-based diversity studies. Nucleic Acids Res. 41:e1.
- Klintzsch T, Langer G, Nehrke G, Mohrholz V, Paul A, Hornick T, et al. 2020. Methane production by three widespread marine phytoplankton species: Release rates, precursor compounds, and potential relevance for the environment. Biogeosciences 17:5163-5180.
- Krom MD. 1980. Spectrophotometric determination of ammonia: a study of a modified Berthelot reaction using salicylate and dichloroisocyanurate. Analyst 105: 305-316.
- Lenhart K, Klintzsch T, Langer G, Nehrke G, Bunge M, Schnell S, Keppler F, 2016. Evidence for methane production by the marine algae Emiliania huxleyi. Biogeosciences 13:3163-3174.
- Lewis CFM, Karrow PF, Blasco SM, McCarthy FMG, King JW, Moore TC Jr, Rea DK. 2008. Evolution of lakes in the Huron basin: Deglaciation to present. Aquat Ecosyst Health Manag 11:127-136.
- León-Palmero E, Contreras-Ruiz A, Sierra A, Morales-Baquero R, Reche I. 2020. Dissolved CH4 coupled to photosynthetic picoeukaryotes in oxic waters and to cumulative chlorophyll a in anoxic waters of reservoirs. Biogeosciences 17:3223-3245.
- McCarthy F, McAndrews J. 2012. Early Holocene drought in the Laurentian Great Lakes basin caused hydrologic closure of Georgian Bay. J Paleolimnol 47:411-428.

- McIntosh JC, Grasby SE, Hamilton SM, Osborn SG. 2014. Origin, distribution and hydrogeochemical controls on methane occurrences in shallow aquifers, southwestern Ontario, Canada. Appl Geochem 50:37-52.
- Mori K, Iino T, Suzuki K, Yamaguchi K, Kamagata Y. 2012. Aceticlastic and NaCl-requiring methanogen *Methanosaeta* pelagica sp. nov., isolated from marine tidal flat sediment. Appl Environ Microbiol 78:3416-3423.
- Murphy J, Riley JP. 1962. A modified single solution method for the determination of phosphate in natural waters. Analytica Chimica Acta 27:31-36.
- Nims RW, Darbyshire JF, Saavedra JE, Christodoulou D, Hanbauer I, Cox GW. 1995. Colorimetric methods for the determination of nitric oxide concentration in neutral aqueous solutions. Methods 7: 48-54.
- Ordonez C, DelSontro T, Langenegger T, Donis D, Suarez EL, McGinnis DF. 2023. Evaluation of the methane paradox in four adjacent pre-alpine lakes across a trophic gradient. Nat Commun 14:2165.
- Patel L, Singh R, Thottathil SD. 2024. Contribution of photosynthesis-driven oxic methane production to the methane cycling of a tropical river network. ACS EST Water 4:2836-2847.
- Repeta DJ, Ferron S, Sosa OA, Johnson CG, Repeta LD, Acker M, et al. 2016. Marine methane paradox explained by bacterial degradation of dissolved organic matter. Nat Geosci 9:884-887.
- Rowe JS. 1972. Forest regions of Canada. Can For Serv Dep Environ. Available from: http://cfs.nrcan.gc.ca/pubwarehouse/ pdfs/24040.pdf
- Saunois M, Stavert AR, Poulter B, Bousquet P, Canadell JG, Jackson RB, Raymond PA, Dlugokencky EJ, Houweling S, Patra PK, et al. 2020. The Global Methane Budget 2000-2017. Earth Syst Sci Data 12:1561-1623.
- Scranton MI, Brewer PG. 1977. Occurrence of methane in the near-surface waters of the western subtropical North-Atlantic. Deep Sea Res 24:127-138.
- Sivan O, Adler M, Pearson A, Gelman F, Bar-Or I, John SG, Eckert W. 2011. Geochemical evidence for iron-mediated anaerobic oxidation of methane. Limnol Oceanogr 56:1536-1544.
- Schagerl M, Künzl G. 2007. Chlorophyll a extraction from freshwater algae a reevaluation. Biologia 62:270-275.
- Stumm W, Morgan JJ. 1995. Aquatic chemistry: chemical equilibria and rates in natural waters. 3rd ed. J. Wiley & Sons, New York.
- Su G, Zopfi J, Yao H, Steinle L, Niemann H, Lehmann MF. 2020. Manganese/iron□supported sulfate□dependent anaerobic oxidation of methane by archaea in lake sediments. Limnol Oceanogr 65:863-875.
- Su G, Zopfi J, Niemann H, Lehmann MF. 2022. Multiple groups of methanotrophic bacteria mediate methane oxidation in anoxic lake sediments. Front Microbiol 13:864630.
- Tang KW, McGinnis DF, Frindte K, Brüchert V, Grossart HP. 2014. Paradox reconsidered: Methane oversaturation in welloxygenated lake waters. Limnol Oceanogr 59:275-284.
- Tang KW, McGinnis DF, Ionescu D, Grossart HP. 2016. Methane production in oxic lake waters potentially increases aquatic methane flux to air. Environ Sci Technol Lett 3:227-233.
- US Environmental Protection Agency (EPA). 2002. Method

- RSKSOP-175: Determination of Henry's Law Constants for Volatile Organic Compounds in Water. EPA/600/R-02/004.
- Verschoor MJ, Powe CR, McQuay E, Schiff SL, Venkiteswaran JJ, Li J, et al. 2017. Internal iron loading and warm temperatures are preconditions for cyanobacterial dominance in embayments along Georgian Bay, Great Lakes. Can J Fish Aquat Sci 74:1439-1453.
- Viollier E, Inglett PW, Hunter K, Roychoudhury AN, Van Cappellen P. 2000. The ferrozine method revisited: Fe(II)/Fe(III) determination in natural waters. Appl Geochem 15:785-790.
- Wang Q, Dore JE, McDermott TR. 2017. Methylphosphonate metabolism by Pseudomonas sp. populations contributes to the methane oversaturation paradox in an oxic freshwater lake. Environ Microbiol 19:2366-2378.
- Wang Q, Alowaifeer A, Kerner P, Balasubramanian N, Patterson A, Christian W, et al. 2021. Aerobic bacterial methane synthesis. P Natl Acad Sci USA 118:e2019229118.

- Wilhelm, E., Battino, R. and Wilcock, R. 1977. Low pressure solubility of gases in liquid water. Chem Rev 77:219-261.
- Xun F, Feng M, Zhao C, Luo W, Han X, Ci Z, et al. 2025. Epilimnetic oligotrophication increases contribution of oxic methane production to atmospheric methane flux from stratified lakes. Water Res 268:122602.
- Yao M, Henny C, Maresca JA, 2016. Freshwater bacteria release methane as a by-product of phosphorus acquisition. Appl Environ Microbiol 82:6994-7003.
- Zastepa A, Miller TR, Watson LC, Kling H, Watson SB. 2021. Toxins and other bioactive metabolites in deep chlorophyll layers containing the cyanobacteria Planktothrix cf. isothrix in two Georgian Bay embayments, Lake Huron. Toxins 13:445.
- Zhu B, van Dijk G, Fritz C, Smolders AJP, Pol A, Jetten MSM, Ettwig KF. 2012. Anaerobic oxidization of methane in a minerotrophic peatland: Enrichment of nitrite-dependent methane-oxidizing bacteria. App Environ Microbiol 78:8657-8665.